The Meteoritical Society

Meteoritics & Planetary Science 44, Nr 4, 471–484 (2009)
Abstract available online at http://meteoritics.org

Infrared spectroscopy of Wild 2 particle hypervelocity tracks in Stardust aerogel: Evidence for the presence of volatile organics in cometary dust

S. BAJT[1, 2*], S. A. SANDFORD[3], G. J. FLYNN[4], G. MATRAJT[5], C. J. SNEAD[6], A. J. WESTPHAL[6], and J. P. BRADLEY[7]

[1]Physics and Advanced Technologies, Lawrence Livermore National Laboratory, 7000 East Avenue, Livermore, California 94550, USA
[2]Present address: DESY, Notkestrasse 85, 22607 Hamburg, Germany
[3]Astrophysics Branch, NASA-Ames Research Center, Moffett Field, California 94035, USA
[4]Department of Physics, SUNY, Plattsburgh, New York 12901, USA
[5]Department of Astronomy, University of Washington, Seattle, Washington 98195, USA
[6]Space Sciences Laboratory, University of California at Berkeley, Berkeley, California 94720–7450, USA
[7]Institute for Geophysics and Planetary Physics, Lawrence Livermore National Laboratory, 7000 E. Ave., Livermore, California 94550, USA
*Corresponding author. E-mail: sasa.bajt@desy.de

(Received 28 August 2007; revision accepted 15 December 2008)

Abstract–Infrared spectroscopy maps of some tracks made by cometary dust from 81P/Wild 2 impacting Stardust aerogel reveal an interesting distribution of organic material. Out of six examined tracks, three show presence of volatile organic components possibly injected into the aerogel during particle impacts. When particle tracks contained volatile organic material, they were found to be -CH_2-rich, while the aerogel is dominated by the -CH_3-rich contaminant. It is clear that the population of cometary particles impacting the Stardust aerogel collectors also includes grains that contained little or none of this organic component. This observation is consistent with the highly heterogeneous nature of collected grains, as seen by a multitude of other analytical techniques.

INTRODUCTION

The Stardust mission flew through the near-nucleus coma of comet 81P/Wild 2 on 2 January 2004, swept up material using aerogel collectors, and returned these samples to Earth on 15 January 2006. Stardust is the first space mission to bring back solid material from a known body other than the Moon. After recovery of the Sample Return Capsule (SRC), the returned material was examined by the members of the Stardust Preliminary Examination Team (PET) with the goal to establish quickly and efficiently the basic nature and amount of the returned samples and disseminate preliminary observations and results. A special issue in *Science* consisting of seven papers (Brownlee et al. 2006; Flynn et al. 2006; Hörz et al. 2006; Keller et al. 2006; McKeegan et al. 2006; Sandford et al. 2006; Zolensky et al. 2006) summarized the main findings of the PET. This paper expands on the distribution of volatile organic components in and around the particle tracks in Stardust aerogel that was briefly reported by Sandford et al. (2006).

The captured material from the Stardust mission is unique and provides new insights into the formation of our solar system. One of the interesting questions that the Stardust samples can address is the origin of primitive organic matter in the solar system. To date, most of our understanding on the astrophysically relevant chemistry of organic molecules has been obtained from telescopic astronomical observations (e.g., Ehrenfreund et al. 1991; Sandford et al. 1991, 1995; Pendleton et al. 1994; Dartois et al. 2004; Moultaka et al. 2004), from laboratory analyses of extraterrestrial materials such as meteorites and interplanetary dust particles (IDPs) (Ehrenfreund et al. 1991; Flynn et al. 2003, 2004; Matrajt et al. 2005), and from laboratory simulations of the formation and evolution of organic molecules in relevant astrophysical environments (e.g., Bernstein et al. 1999, 2002; Mennella et al. 2002; Muñoz-Caro et al. 2002). Such studies have yielded important information about the nature of extraterrestrial organics. However, remote observations are limited in the information they can provide. In addition, collected samples in the form of meteorites and IDPs are all "orphans," in the sense that they cannot be associated with specific parent bodies, making it somewhat difficult to put findings from them in proper context. Thanks to Stardust, we now have cometary dust from a known comet (comet 81P/Wild2), that is thought to have undergone little parent body processing

(Brownlee et al. 2006; Sandford et al. 2006), and which has suffered minimal space exposure prior to collection (Brownlee et al. 2006). This material provides a unique opportunity to examine primitive solar system organics.

Comet 81P/Wild 2 is thought to have formed in the outer region of our planetary system, after which it was ejected into the Kuiper belt (Brownlee et al. 2006). It was selected as the target comet for the Stardust mission for several reasons. First, it is currently in a favorable orbit for relatively low velocity flybys with small spacecraft (Brownlee et al. 2003). Thus, the dust hit the aerogel with "relatively" low velocity of 6.1 km/s. Second, it has only been in its current orbit since September 1974 and has therefore made only a modest number of passes close to the Sun. Prior to 1974, when the comet had the close encounter with Jupiter, that injected the comet into its current orbit, it was in an orbit that fell entirely outside the orbit of Jupiter. This makes Wild 2 a good candidate for the collection of early solar system materials that have undergone relatively little parent body processing. The captured particles ejected by the comet were largely associated with two of the many jets seen to come from the nucleus (Yelle et al. 2004) and are expected to be representative of the interior of the comet rather than its surface (Brownlee et al. 2006). These particles were captured in low density aerogel at a velocity of 6.1 km/s relative to the spacecraft.

Aerogel is an extremely low-density, microporous silica material that proved efficient capture of small particles at speeds of 6–7 km/s (Tsou 1995; Brownlee et al. 2003; Tsou et al. 2003; Burchell et al. 2006). The aerogel in the cometary tray had a density gradient with the lowest density near the front surface of the tiles in order to provide small particles with the gentlest possible deceleration, and increasing density with depth to provide greater stopping power for larger grains. The cometary aerogel tiles were 3 cm thick and were predicted to stop grains as large as ~200 μm in diameter (depending on their composition and structure).

This paper reports our observations of labile organics distributed in aerogel along and around some particle impact tracks. The measurements were performed with synchrotron-based infrared microspectrometers with ~1000 times higher flux and ~100 times better signal/noise ratio as compared to conventional laboratory infrared spectrometers. Infrared spectroscopy is a powerful technique for direct observations of dust and ice composition in many astrophysical environments, including comets, and allows for direct comparison with extraterrestrial and standard materials analyzed in the lab. We tried to address the following questions associated with these materials, although with somewhat limited success: 1) Did we capture volatiles from Wild 2 cometary dust? 2) Did they change during the capture in aerogel and how? 3) What can we learn about the original chemistry of impact particles from these data?

The captured particles are believed to be exposed to space for a maximum of a few hours after release from the comet and therefore some volatile components, such as ices and volatile organics, could potentially have been present in the impactors, especially in larger particles (Brownlee et al. 2006). However, it is expected that due to hypervelocity impact, all particles experienced some modification during the capture. Also, Stardust aerogel tiles contain up to a few percent indigenous carbon (Tsou et al. 2003), largely in the form of Si-CH_3 groups, but -CH_2-, -O-CH_3, and other groups are also present. This results in several complications for the work reported here. First, this carbon produces a background of infrared absorption that must be accounted for when examining the spectra of material still in the aerogel. Second, this carbon represents a reservoir of material from which other organics might be made during the impact process. These issues are discussed in more detail in the body of the paper.

MATERIALS AND METHODS

Sample Preparation

"Keystone" samples, i.e., aerogel wedges containing whole particle tracks along with the original surface of the collector tile were prepared using a technique developed at the Space Sciences Laboratory, U. C. Berkeley (Westphal et al. 2004). The aerogel is cut by repetitive "poking" of micro-needles held by computer controlled micromanipulators attached to the stage of the extraction microscope. First, an angled cut is made which undercuts the deepest feature of a particular impact; then a vertical cut is made around the impact. The resulting wedge-shaped block of aerogel (a "keystone") contains the entire impact track and the terminal particles. The keystone is then removed from the collector using silicon micro-forks that are inserted into premachined holes in the keystone at a location to the side of the track in the tile's original surface. An example of a "keystone" with a bulbous shaped track is shown in Fig. 1. In some cases, the track was sliced into multiple cross sections. These specialized samples are prepared by laying a keystone on its side and using the same aerogel cutting tools to dissect or slice wafers of the track bulb. Such thin aerogel slices are then sandwiched between two standard transmission electron microscope Cu grids.

Methods

The results presented in this paper were obtained at two synchrotron based Fourier transform infrared (FTIR) microscopes, the National Synchrotron Light Source (NSLS) at Brookhaven National Laboratory (Upton, NY) and the Advanced Light Source (ALS) at Lawrence Berkeley National Laboratory (Berkeley, CA). These synchrotron

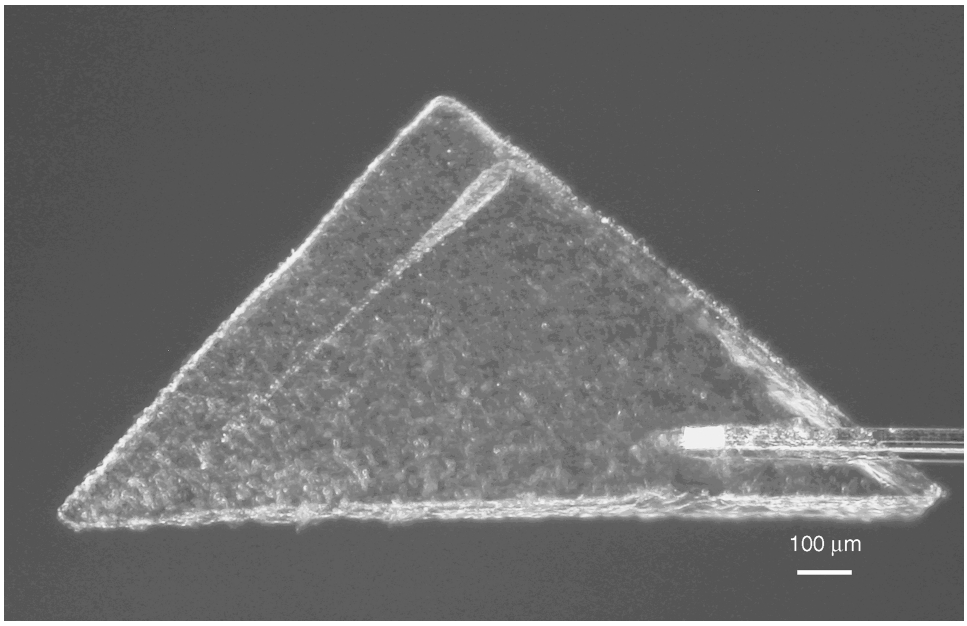

Fig. 1. Track C2115,22,20. The original aerogel surface exposed to the comet is shown on the right hand side. The linescans in Fig. 3 were perpendicular to the track, e.g., parallel to the original aerogel surface.

sources, which are about two to three orders of magnitude brighter than a blackbody source, provide high brightness (power/unit area) beams, and enable imaging with diffraction limited beam spots. This yields the advantage of very high sensitivity compared to conventional laboratory IR spectrometers and allows one to do molecular and compositional analysis in very small spots with high signal-to-noise ratios (Holman and Martin 2006). Infrared spectroscopy also has the advantage that it is a very noninvasive technique that is sensitive to chemical functional groups in molecules and can therefore provide considerable information about the chemical nature of a sample without altering or destroying it.

Both systems consist of a source of infrared light (the synchrotron), an interferometer, a microscope equipped with an infrared detector, and a data recording and analysis system. The ALS beamline 1.4.3 is equipped with a ThermoNicolet Magna 760 FTIR bench and a SpectraTech Nic-Plan IR microscope. The FTIR bench used a KBr beam splitter and the transmitted light was collected with a Mercury Cadmium Telluride (MCT-A) detector between 650 and 4000 cm^{-1} with 4 cm^{-1} spectral resolution. Spectra were normalized to the spectrum of the beam through the air and typical collection times on keystone samples were between 6 and 60 seconds per position. Aerogel keystones held with silicon microforks were attached to a specially made substrate holders that fit into the microscope slide holder and were placed directly under the microscope objective. In this way, the sample could be moved under the microscope with submicron precision utilizing a software stage control while the synchrotron beam remained fixed. Hence, the maps obtained at the ALS were collected as raster scan where the whole spectrum (from 650 to 4000 cm^{-1} range) was recorded for each individual point in the map. Optical and infrared beams were aligned prior to each session and after each synchrotron beam refill, which typically occurs every 8 hours, in order to have a perfect match between optical and infrared images.

The NSLS beamline U10 is built on a bending magnet port of the VUV ring (Carr et al. 1999). The beamline delivers diffraction limited beam and is optimized for infrared microscopy/microspectroscopy. The NSLS measurements reported in this paper were made on a Nicolet Continuum FTIR spectro-microscope, equipped with a fixed Ge/KBr beam splitter, two Schwarzchild all-reflecting objectives (15X and 32X), automated X-Y scanning stage for spectroscopic mapping with 1 μm step resolution and two MCT detectors that cover the wave number range from 450 to 4000 cm^{-1}. The analyses were made by obtaining an air background, then measuring the absorption of the keystone containing the particle track, using analysis spots of 10 μm × 10 μm to 20 μm × 20 μm.

Contamination Control and Assessment

After extensive laboratory experiment testing of different capturing materials it became clear that the capturing material for the Stardust mission had to satisfy at least two conditions: 1) it had to be of sufficient low density to gradually decelerate and capture the particles, and 2) it had to have high surface area to adsorb any volatiles. Silica-based aerogel was proposed to be used due to its transparency, low density, and fine mesostructure (Tsou 1995; Tsou et al. 2003). The Stardust silica aerogel was fabricated by the two-step sol-gel process followed by high temperature supercritical point extraction

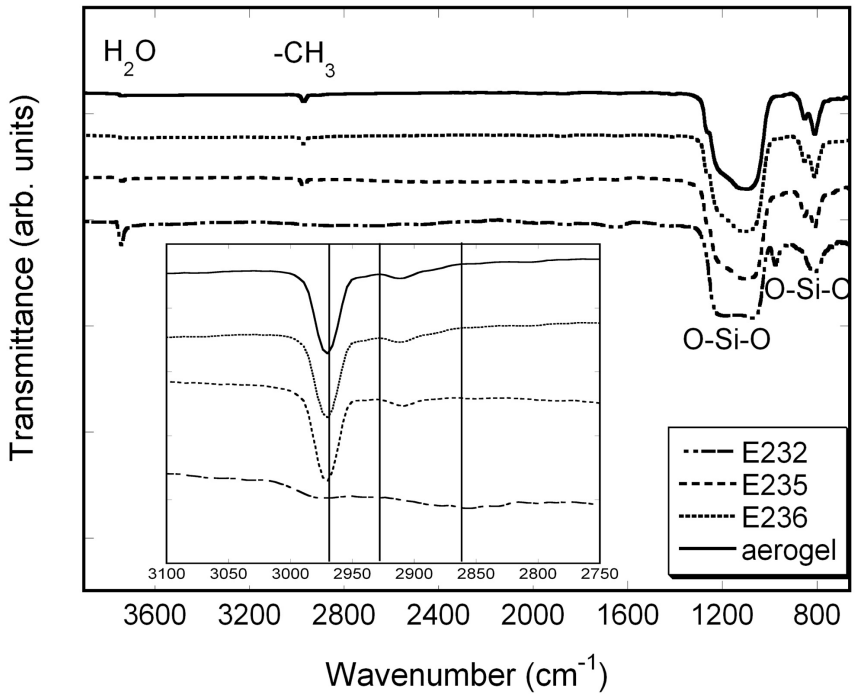

Fig. 2. Infrared spectra of three flight spare aerogel tile batches, E232, E235, and E236 and a control aerogel sample that flew on Stardust but was not exposed to the comet. All are showing a strong peak centered at 1125 cm^{-1} (O-Si-O), peak at 810 cm^{-1} (O-Si-O), and a small shoulder peak at 975 cm^{-1} (Si-OH), and some are showing 2970 cm^{-1} (-CH_3) and 3740 cm^{-1} (-OH in water or Si-OH stretch). The aerogel tile batches were prepared in 1998 (together with control aerogel sample), stored in dry nitrogen and never left the Earth. All the spectra are plotted on the same scale (0 to 100% transmission) but are offset for better visibility. One tick on the y-scale corresponds to 50% transmission. The insert shows a close-up between 3100 and 2750 cm^{-1}.

and a mild vacuum-bake cycle at 300 °C (Tsou 1995; Tsou et al. 2003). The Stardust cometary cells have several formats—some cells consists of three density layers with the lowest density (5 mg/ml) being on the top surface of the aerogel cells and the highest density (50 mg/ml) on the bottom, while others have continuous density gradients, but still with the lowest density aerogel near the surface. The density gradient aerogel does not compromise sample survival efficiency while at the same time decreases the total thickness of the cells and increases the maximum particle size that can be captured. Due to its high surface area, aerogel is also ideal medium to adsorb any volatiles entrapped in the dust particles. FTIR spectroscopy was one of the techniques that measured aerogel organic contamination prior to launch and it was established that the initial aerogel contained aliphatics, chiefly in the form of -CH_3 groups. It was also demonstrated that mild heating substantially reduced the residual organics. Prior to flight, all aerogel was heated to 300 °C for 72 h to reduce organic contamination. The carbon content after the heating was typically less than a few percent by mass (Tsou et al. 2003; Sandford et al. 2006). NMR studies of aerogel tiles treated in this manner confirm that the remaining carbon is largely in the form of Si-CH_3 groups, but lesser amounts of -CH_2- and other groups are present as well. This residual contaminant carbon produces infrared background absorption that must be accounted for in IR studies of Stardust materials still in aerogel and represents a reservoir of material that could potentially be converted to other forms during particle impacts.

Figure 2 shows infrared spectra of seven year old aerogel samples from three different aerogel batches (E232, E235, E236) prepared at the same time as the Stardust aerogel. These aerogels never left the Earth and were stored for the last 7 years in dry nitrogen. They provide a baseline for initial Stardust aerogel composition. We notice subtle differences among them, in particular in the strengths of the -OH and -CH_3 bands. All three samples show peaks due to O-Si-O bonds characteristic for aerogel, a broad peak between 1100–1200 cm^{-1} and a peak at 810 cm^{-1}. Sample E232 also displays peaks at 3742 cm^{-2}, 1649 cm^{-1}, and 975 cm^{-1}, which are attributed to -OH groups. A sample from another batch, E235, shows these same peaks, but their intensity is weaker as compared to E232. This sample has an additional peak at 2971 cm^{-1}, attributed to -CH_3. In the third sample, E236, we find only -CH_3 peak at 2971 cm^{-1} and a very weak peak associated with -OH. These measurements indicate that the aerogels made in different batches can be distinguished based on their FTIR spectra. They also confirm that some initial contamination of -OH and -CH_3 is present. The fourth spectrum in Fig. 2 is a control sample, aerogel that

flew on Stardust spacecraft but *was not* exposed to the comet. When comparing it with other aerogel samples that did not fly on the spacecraft we observe the same type of contaminants, characterized by a peak at 2971 cm^{-1} (-CH_3) and/or at ~3742 cm^{-2} (-OH). Hence, from a FTIR point of view long exposure to space and flying on the spacecraft did not further contaminate the aerogel. Nonetheless, it is clear that care must be taken to account for absorptions due to indigenous aerogel carbon when interpreting spectral data of samples collected in aerogel.

RESULTS

We will first describe results obtained with NSLS FTIR microscope. Only two tracks, tracks C2115,22,20 and C2115,23,21 (from the same cell) were examined with the NSLS FTIR microscope. Both tracks showed a fairly typical "ginseng" shape, and had comparable lengths of ~900 μm (Fig. 1 shows one of them, C2115,22,20). We took a series of spectra that traversed perpendicularly across both tracks at regular intervals, and normalized each spectrum to the spectrum of air.

One of the tracks (C2115,23,21) showed no variation in the obtained infrared spectra independent of the location examined on the aerogel keystone. This implies that, within the sensitivity limits of the measurement, the particle lost little or no organics along the track during impact. There is also no evidence, again within the sensitivity limits of the measurement, that the impact process created new organic species from carbon indigenous to the aerogel.

In contrast, the second track (C2115,22,20) showed significant spectral variation with position examined in the aerogel keystone. Figure 3 shows the 3100–2750 cm^{-1} (3.23–3.64 μm) C-H stretching region for positions along the "south" traverses from the center of this track. The north traverses (not shown) is very similar. Since the spectra are normalized to the air, the absorption features consist of a combination of any cometary sample present and the aerogel. Cometary sample is therefore indicated by the presence of excess absorption over that seen for the aerogel alone. As mentioned before, organics in the original aerogel are dominated by -CH_3 groups, whose most obvious absorption falls near 2970 cm^{-1} (see Fig. 2, bottom spectrum of Fig. 3, and Sandford et al. [2006]). Added material is manifested by the presence of additional absorption near 2985 and 2935 cm^{-1} (highlighted by the dashed lines in Fig. 3). The feature at 2935 cm^{-1} falls at a location characteristic of the asymmetric C-H stretching vibration of aliphatic -CH_2- groups. The feature at 2985 cm^{-1} might be explained by the presence of olefins. This identification is somewhat problematic since aerogel also has an absorption peak at this position. However, this band grows in the spectra in Fig. 3 as one approaches the track center, indicating some additional material is present. We note that olefinic bonding is seen in the C-XANES spectra of some Stardust organics (Sandford et al. 2006; Cody et al. 2008). It is clear from Fig. 3 that the material that produces these two bands is not restricted solely to the confines of the physical impact track, but extends outward beyond the nearest edge of the track (a similar dispersion is seen on both sides of the track).

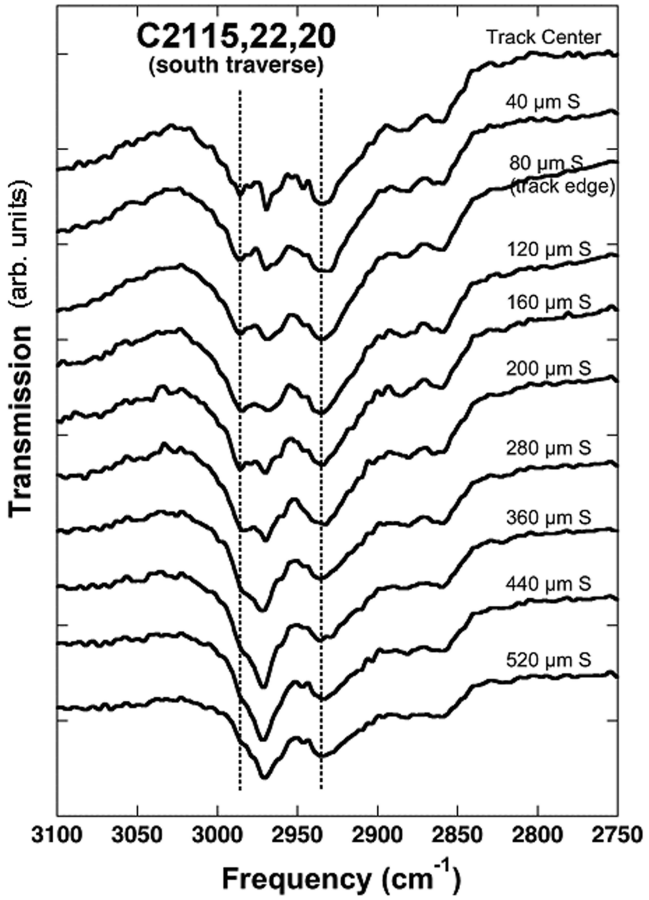

Fig. 3. Details of infrared spectra taken from track C2115,22,20. The spectra were taken every 40 μm starting from the track center and are displayed offset for better visibility. Dashed lines at 2985 and 2935 cm^{-1} mark spectral positions where excess absorption is seen as one approaches the center of the track. It is also clear that the material that produces these two bands is not restricted solely to the confines of the physical impact track, but instead extends outward beyond the nearest edge of the track (the physical edge of the track is at the 80 μm S position). A similar dispersion is seen on both sides of the track.

These results are consistent with the spectral interpretations of organics in a number of other Stardust samples that indicated that many of the cometary organics, when present, contain abundant -CH_2- groups (Keller et al. 2006; Sandford et al. 2006). Indeed, the captured cometary materials tend to show considerably higher -CH_2-/-CH_3 ratios than that seen in the diffuse interstellar medium and in meteorites. In this respect, the cometary samples resemble IDPs, which also show large -CH_2-/-CH_3 ratios (Flynn et al. 2003, 2004; Matrajt et al. 2005).

These results made it apparent that tracks differ in the amount of organics they contain and that IR spectroscopy of individual points along an impact track does not necessarily

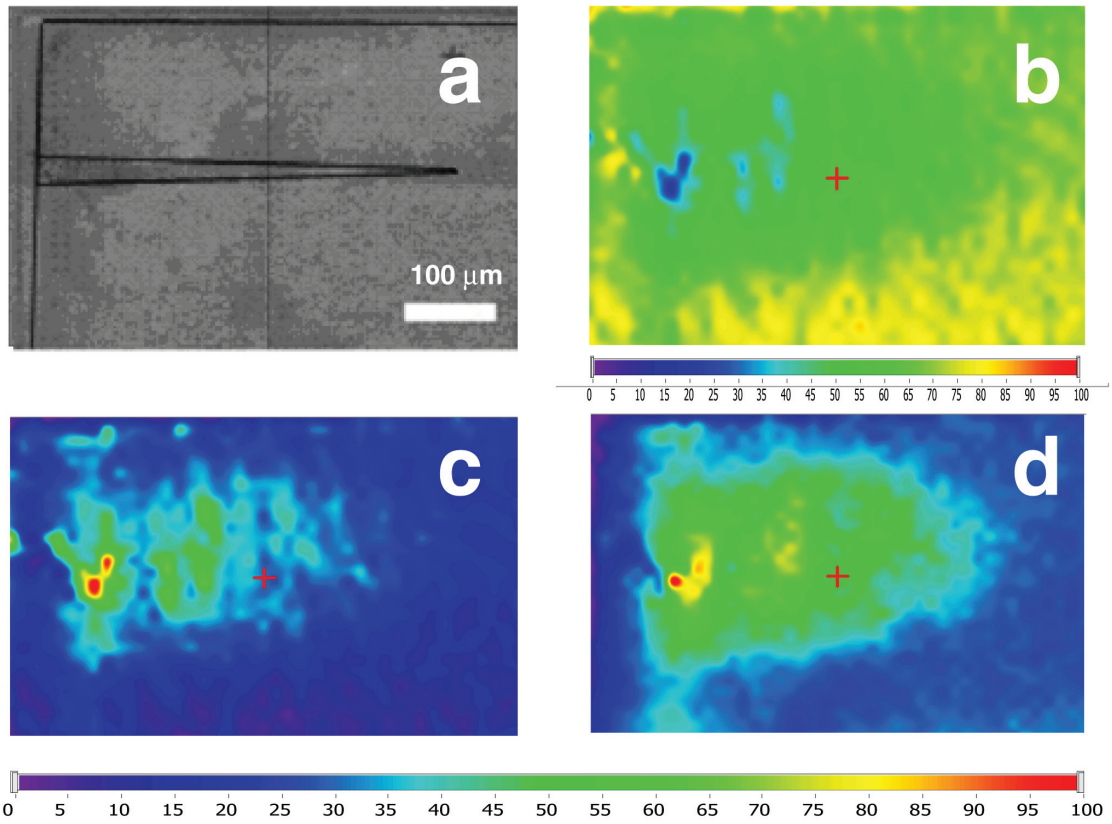

Fig. 4. a) Optical image showing the edges of the keystone and the approximate outline of the track C2009,7,62. The original surface exposed to the comet is on the left. b) Raw transmission map (x, y, full spectrum) for the wave number position of 2926 cm^{-1}. The scale bar is from 0 to 100% transmission. c) Absorbance map for the same wave number as in Fig. 4b. The scale bar plotted on the bottom goes from 0 to 100% absorbance. d) Background corrected absorbance map for the aforementioned wave number. Same scale bar as in Fig. 4c. The dimensional scale bar is the same in all four images (see 100 μm bar in Fig. 4a).

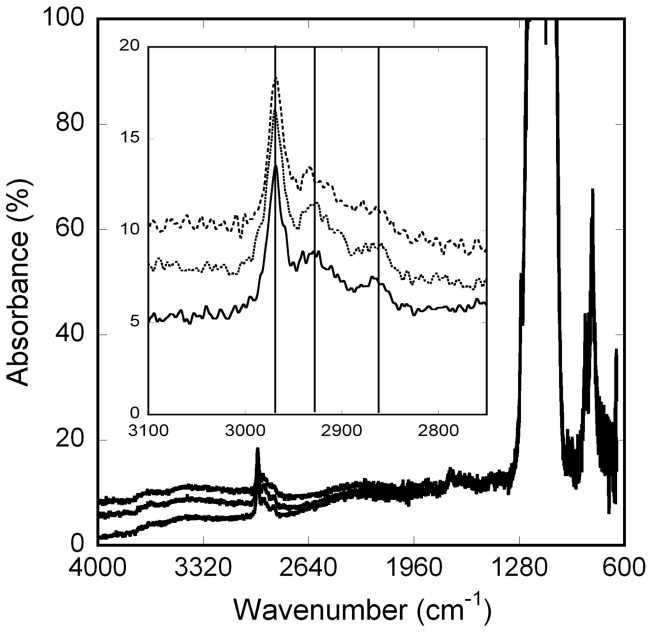

Fig. 5. Spectra from three different locations in the "clean area" aerogel, far away from the particle track with an insert showing a close-up region of 3100 to 2750 cm^{-1}. The data are plotted as absorbance spectra in %.

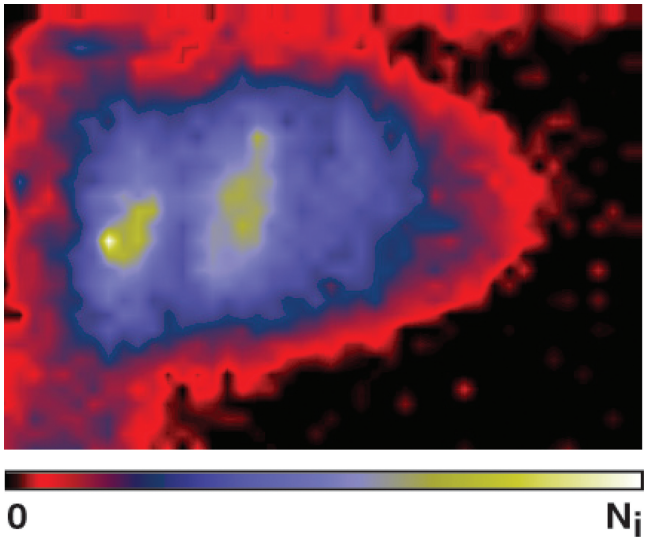

Fig. 6. Aerogel corrected map from Fig. 4 (C2009,7,62). The black color corresponds to 0 and white corresponds to maximum density of functional group (in this case -CH_2-). The mapped area is identical to the one shown in Fig. 4 (approximately 650 × 450 μm^2).

give a complete assessment of the total organic inventory of the impacting particles. Spectral 'maps' of entire tracks need to be collected if a more complete assessment of the organics associated with a given impacting particle is to be obtained. Fortunately, several spectral maps of tracks were measured during PE at the ALS beamline at Lawrence Berkeley National Laboratory.

Data from Spectral Maps

Here we will present infrared spectral maps of four keystones that were measured in transmission mode at the ALS FTIR spectro-microscope. Because of extremely low density (~5 mg/cm^3) of Stardust aerogel, the few hundred micron thick keystones are still transparent across the entire spectral region of interest (except for a few data points near ~1000 cm^{-1}). This means that the aerogel peak at 800 cm^{-1} was not saturated and could be used for background correction as described below. Maps were collected as raster scans, where a full FTIR spectrum was measured from 650 to 4000 cm^{-1} at each point in the map. Excess absorption over that seen in aerogel far from the track at the vibration frequencies of particular bonds reveals material not present in the original aerogel. In the following we will describe in detail the data collection and processing procedures and show them step by step on one example, an IR map of particle track C2009,7,62. The optical image of the mapped area is shown in Fig. 4a. For better visibility we outlined the edges of the keystone and indicated the track entrance and direction with black solid lines. The original aerogel surface exposed to the comet is on the left hand side (Fig. 4a).

The data set for each point in infrared maps included x and y coordinates and a full FTIR spectrum (x, y, full spectrum). The infrared maps were collected in transmission and normalized to the air spectrum, same setup but no sample under the beam. From these raw spectra (Fig. 4b shows the distribution of a peak at 2926 cm^{-1}) we calculate the optical depth of the observed absorbance features [i.e., $\tau = -\ln(I/I_o)$]. Figure 4c shows as an example the depth of the absorbance feature at 2926 cm^{-1}, characteristic of -CH_2- band. As shown in Fig. 2 this absorbance feature was not present in the original, unexposed aerogel. The background corrected peak value for all absorbance features of interest results in multiple maps, (x, y, value) where the value corresponds to the background corrected absorbance of a particular band. Figure 4d shows background corrected absorbance map for 2926 cm^{-1} band.

Next, we make a thickness and composition correction due to aerogel present in each point. This is done by first extracting the background corrected peak values for all functional groups of interest in a point far away from the track ("clean aerogel") and then correcting each individual pixel in our maps for this aerogel contribution.[1] Absorbance spectrum of a "standardized" aerogel (aerogel far away from the track) is shown in Fig. 5. In fact, several spectra of standardized aerogel are displayed to show that the spectra of "clean aerogel" within the same keystone are very similar and do not contribute more than few % error in the final calculations, i.e., our maps are not sensitive to the particular "clean aerogel" spectrum used. The insert shows a close-up spectrum of the region of interest between 3100 and 2750 cm^{-1}. After correcting each pixel for the aerogel contribution we obtain absorbance maps of excess materials beyond those of the original aerogel. Figure 6 shows such an absorbance map of added -CH_2- material not present in the original aerogel. This is different to results in Fig. 4d where the map was not yet corrected for thickness and aerogel composition yet.

To further calculate the number of functional groups the following steps were taken. The absorption values, τ, from all the pixels within the map, showing excess absorption of a particular functional group, were multiplied by the relevant feature's width and divided by its intrinsic band strength as shown in Equation 1.

$$N(\text{groups/cm}^2) = \frac{\tau_i \Delta\upsilon}{A} \quad (1)$$

where τ_i, is the depth of the absorbance feature for i-th pixel, $\Delta\upsilon$ is the spectral width of the feature, and A is the intrinsic band strength for the function group. The τ_i, and $\Delta\upsilon$ values were determined experimentally from the maps (Table 1), while literature values were used for intrinsic band strengths, A (Wexler 1967; Sandford et al. 1991). Using this procedure we estimated the number of functional groups of each component present in the maps by summing all the values within the measured area. The results are listed in Table 1.

Four tracks (C2009,4,59; C2009,7,62; C2009,3,58; C2009,6,61) and two wafer slices (C2009,5,60; C2009,2,57) were mapped in this study. All these samples come from the same cell, C2009. After the data collection of the maps on the wafer slices it became obvious that the mapped area did not extend far enough from the center of the track to capture "clean aerogel", i.e., the extended "plumes" of organic material appear to extend out to the very edge of the cut wafers. For this reason, we do not include the data from wafer slices, but instead concentrate only on the full tracks. Three of these samples (C2009,4,59; C2009,7,62; C2009,3,58) show evidence of additional material extending beyond the tracks, similar to aforementioned data from Track C2115,22,20. As an example, spectra collected at different distances from the track in sample C2009,7,62, are plotted in Fig. 7. Transmission spectra (same y scale in percent) have been offset for better visibility. The intensities of the absorbance

[1]Because a peak due to O-Si-O vibration at ~1100 cm^{-1} (aerogel) is sometimes saturated, we have used another characteristic, weaker peak near ~800 cm^{-1} for normalizing the aerogel spectral contribution.

Table 1. *The intrinsic band strengths values, A, are given in cm per functional group (Sandford et al. 1991).

	C2009,7,62	C2009,4,59	C2009,6,61	C2005,5,60
$\Delta\upsilon_{-CH2-}$ (cm^{-1})	20	20	18	20
$\Delta\upsilon_{-CH3}$ (cm^{-1})	20	20	22	24
$\Delta\upsilon_{C=O}$ (cm^{-1})	28	32	30	n.d.
A_{-CH2-}*	8×10^{-18}	8×10^{-18}	8×10^{-18}	8×10^{-18}
A_{-CH3}*	1.2×10^{-17}	1.2×10^{-17}	1.2×10^{-17}	1.2×10^{-17}
$A_{C=O}$*	1.7×10^{-17}	1.7×10^{-17}	1.7×10^{-17}	1.7×10^{-17}
N_{-CH2-}**	1.2×10^{14}	5.2×10^{14}	1.9×10^{13}	7.9×10^{13}
N_{-CH3}**	6.2×10^{13}	2.6×10^{14}	1.0×10^{13}	1.1×10^{14}
$N_{C=O}$**	6.4×10^{13}	3.1×10^{14}	1.9×10^{13}	n.d.

**N is the number of functional groups in each track. The error bars on N numbers for C2009,7,62 and C2009,4,59 are 10% and for C2009,6,61 and C2009,5,60 are about 50%.

Table 2. List of all examined tracks. Comparison based on their lengths, angle of incidence, and presence of volatile components.

Sample name	Approx. track length (μm)	Angle of incidence	Excess volatile component
C2009,3,58	256	Off-normal	Yes
C2009,4,59	320	Off-normal	Yes
C2009,7,62	500	Ambiguous	Yes
C2115,22,20	900	Normal?	Yes
C2115,23,21	900	Normal	No
C2009,6,61	1480	Off-normal	No

peaks (-CH_2-: 2926 cm^{-1}, -CH_3: 2963 cm^{-1}, C=O: 1720 cm^{-1}) decrease with the distance from the track, while the aerogel peak at 800 cm^{-1} (not shown) remains constant. However, just as was observed in the NSLS data from track C2115,22,21, we also measured tracks with no variation in peak intensities as a function of the distance from the track. Track C2009,6,61 (Fig. 8) is an example where peak intensities do not change as a function of distance. In fact, the spectra taken from this sample match the spectrum in Fig. 7 taken 400 μm from the track center, in "clean" aerogel.

Figure 9 shows fully corrected absorbance maps from sample C2009,4,59, for -CH_2- (Fig. 9a), -CH_3 (Fig. 9b), and C=O (Fig. 9c) bands calculated as described above. The optical image with keystone edges and track outline is shown in Fig. 9d. The two vertical black lines in Fig. 9d are due to stitching multiple optical microscopy images. The same false color bar was used for all three absorbance maps, -CH_2-, -CH_3, and C=O groups with black corresponding to 0 absorbance and white to the maximum number of functional group/cm^2. It is obvious that the -CH_2- band is very strong within <50 μm from the track walls and decreases rapidly with the distance from the track. It reaches the background level, present in the original aerogel, within few hundred μm from the track. The maximum absorbance of the -CH_3 band is about half of that observed for -CH_2- band but the outline of the area enriched with this compound matches that of the -CH_2- distribution. The third absorbance map, showing the distribution of the C=O band,

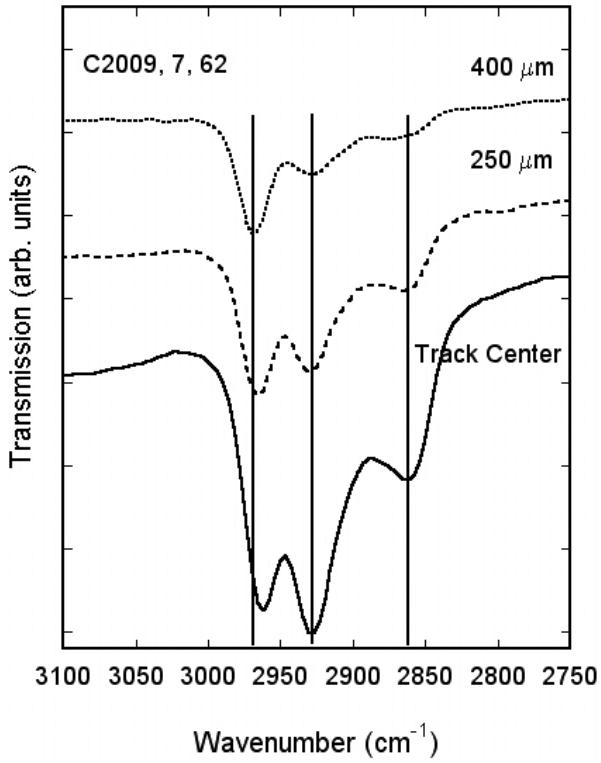

Fig. 7. Details of infrared spectra taken from track C2009,7,62. All three spectra are plotted on the same scale (0 to 100% transmission) but are offset for better visibility. One tick interval on the y-axis corresponds to 10% transmission.

shows very weak absorption compared to -CH_2- absorbance map, but matches the distributions of the other spectral components in and around the track. These differences might be related to different volatility (diffusivity) of these components, with -CH_2- being the least volatile and C=O and -OH (not shown) the most volatile.

The aforementioned C2009,6,61 track (Fig. 8) showed no change in peak intensities as a function of distance from the track. Hence, it is not surprising that the absorbance maps obtained from this sample (Fig. 10) look more uniform than in Fig. 9. This map was collected with larger steps and has

therefore lower resolution than the map shown in Figs. 6 or 9. The same false color bar is used for all three absorbance maps, with black representing 0 and N_i representing the maximum number of functional groups/cm^2 in these maps. The absorbance maps of -CH_2- (Fig. 10a), -CH_3 (Fig. 10b) and C=O (Fig. 10c) are displayed, respectively. Small excesses in -CH_2-, and possibly -CH_3 in few individual pixels (40 × 8 μm) may correlate with small organic-rich particles primarily seen at the entrance of the track (left side of the images) but could also indicate surface contamination. The optical image with the track outline is displayed in Fig. 10d.

Hence, some tracks show no distributed volatile component. The lack of additional organic material in track C2009,6,61 also suggests that the new features seen in other tracks are not due solely to the reprocessing of carbon indigenous to the aerogel by the particle impact. If impact processing produced these features from aerogel carbon, one would expect to routinely see them around tracks. The degree to which aerogel carbon might be converted to other forms clearly depends to some degree on the initial mass, density, and composition of the particle. A proper impact analysis to study the effects of these parameters on possible impact processing is clearly beyond the scope of this work. However we would note that particles producing tracks of similar dimensions will have deposited similar energy densities into the aerogel and would likely experience comparable degrees of processing. While we have only examined a limited number of tracks, our results are not consistent with the idea that all the excess organics are due to impact processing of aerogel carbon.

Table 1 lists the total number of functional groups in a track for the three functional groups -CH_2- (for example, N-CH_2), -CH_3 and C=O found in aforementioned maps. We examined the ratios of -CH_2-/-CH_3, -CH_2-/C=O, -CH_3/C=O in "organic-rich" tracks (C2009,7,62 and C2009,4,59) and in "organics-poor" tracks (C2009,5,60; C2009, 6, 61). In "organic-rich" tracks the -CH_2-/C=O ratios range between 1.7 and 1.9, the -CH_3/C=O ratios between 0.8 and 0.95, while the -CH2-/-CH_3 ratios are basically the same (2.0). The -CH_2-/-CH_3 ratios in the samples with small amounts of extra material ("organics-poor") were 0.7 versus 1.8. We estimate the ratios -CH_2-/C=O and -CH_3/C=O in the track C2009,6,61 to be 2.3 and 1.3, respectively.

DISCUSSION

Infrared spectroscopy is used primarily as a qualitative, fingerprinting technique. From the baseline aerogel spectra we identified -CH_3 as the main organic contaminant in the original collector tiles (Fig. 2). The observed presence of extra absorption outside the confines of the physical impact track implies that either (i) some of the organics in the original particle were volatilized and diffused into the local aerogel during impact or (ii) that heat or shock from the impact altered carbon in the aerogel near the track.

The interaction between the impacting cometary grains, in particular organic-rich particles, and aerogel and its indigenous carbon is still largely unexplored area. The impact and deceleration of particles into Stardust aerogel at 6.1 km/s involves the dissipation of considerable energy and thermal processing of local aerogel (i.e., Stratton and Szydlik 1997). This energy has the potential to process carbon indigenous to the aerogel as well as alter any organics originally present in the impactor.

Work in which high power laser shots were used to simulate hypervelocity impacts in aerogel has demonstrated that some of the indigenous carbon in these aerogels can be converted into a fairly simple population of light weight polycyclic aromatic hydrocarbons (PAHs) (Spencer and Zare 2007). However, the amounts of material converted in this manner would be too small to be detected by the IR techniques described here (Sandford and Brownlee 2007). Thus, the conversion of aerogel C into aromatic materials does not seem to be very efficient. However, the issue of the conversion of aerogel C into aliphatic materials is less constrained. Again, the fact that some of our tracks show the presence of new, extended distributions of organics and others do not, and that our maps do not show losses of -CH_3 comparable to the excess -CH_2- we see, suggests that the conversion of aerogel C cannot be the sole, or even main, source of the organic track halos we observe around some tracks. Nonetheless, the possibility (indeed, likelihood) that at least *some* of the organics found in tracks have an origin in the conversion of carbon indigenous to the original aerogel should be constantly kept in mind. Only future test shots, preferably with completely organic free impactors, will allow this issue to be better constrained.

We favor the interpretation that the organic halos are largely associated with materials indigenous to the cometary particles because data taken across similar length tracks, for example C2115,23,21 and C2115,22,20 (Fig. 3) show C-H stretch spectral profiles that imply very different degrees of added absorption. If the spectral differences seen in the track C2115,22,20 traverse were due to impact processing of carbon indigenous to the aerogel, we would have expected to see similar processing around all tracks, including track C2115,23,21, which showed no spectral variations with position around the track. This suggests that the additional organics seen in and around track C2115,22,20 represent a component associated with the impacting particle that made this track. Similar results were observed in C2009,7,62; C2009,4,59 (Figs. 7 and 9) and C2009,6,61 (Figs. 8 and 10) that exhibit significantly different amounts and distribution of extra volatile material. These variations are consistent with the overall heterogeneity of the organic content of different Wild 2 grains as observed by a variety of other analytical techniques (see, for example, Sandford et al. 2006; Cody et al. 2008; Matrajt et al. 2008; Rotundi et al. 2008; Spencer et al. 2009; Clemett et al., Forthcoming). Such

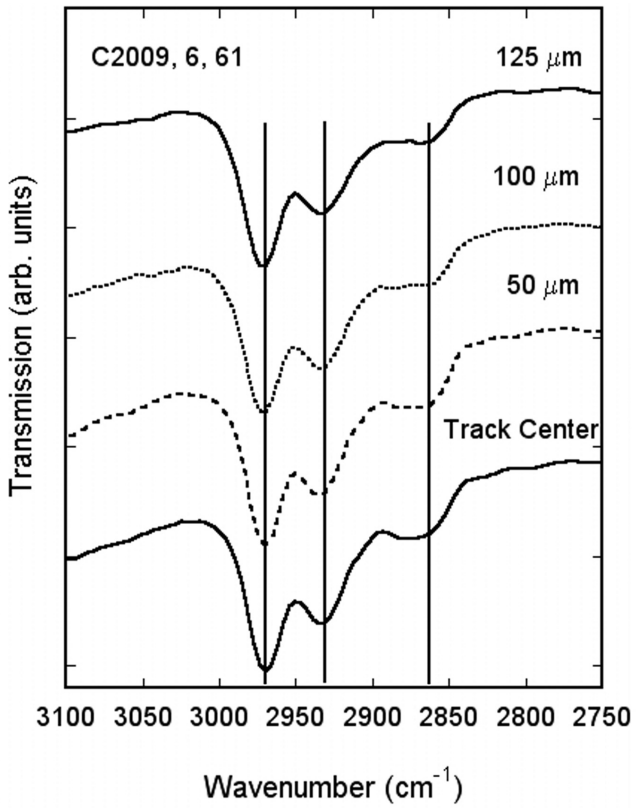

Fig. 8. Data taken from track C2009,6,61 show no change in infrared spectra as a function of the distance from the track. All the spectra are plotted on the same scale (0 to 100% transmission) but are offset for better visibility. One tick interval on the y axis corresponds to 10% transmission.

variations would be difficult to understand if all the organics were simply due to impact processing of aerogel carbon.

Off-normal tracks could also indicate particles that either bounced off or were diverted by the Whipple shield before impacting aerogel (Westphal et al. 2008). This would lower their impact velocity and/or potentially contaminate them with Whipple shield material (Kapton). There is a lack of data in calibration rates of organics as a function of impact velocity and no data exist in the distribution of organics after the impact as taken here with FTIR microscope. Figure 11 shows a spectrum of polyimide (Kapton) and compares it to a spectrum from an organic rich region in Stardust aerogel. The two spectra are clearly different. In particular, strong peaks between 1600–1300 cm^{-1} in the Kapton spectrum are missing in the Stardust aerogel spectrum. Thus, the additional material can not simply be explained with Kapton contamination. Additional support for this explanation is the presence of extra organics in both off-normal and normal incidence tracks and the fact that these organics are similar. This indicates the same (similar) source for these materials. If the source was Kapton from the Whipple shield, then the normal incidence tracks should have no additional material and/or this material should be different to the off-normal incidence tracks. This is clearly not the case.

Assuming the additional volatile organics-rich material is of cometary origin it is meaningful to estimate the amount of carbon (organics) in the impacting particles. Our attempt to calculate the number of functional groups per track from the FTIR maps is listed in Table 1. The samples with added volatile organics-rich components (C2009,7,62; C2009,4,59) have on average about and order of magnitude higher number of functional groups as the samples with no additional materials (C2009,6,61; C2009,5,60).

The organics studied in this work are diffuse, presumably moderately volatile, materials seen along and around the tracks, not those that are associated with terminal particles. These materials may differ significantly from the organics seen in IDPs collected in the stratosphere since IDPs will likely have lost these more volatile materials (if they ever had them) during transit from their parent body to Earth and during atmospheric entry. A more apt comparison to IDPs might therefore be made to terminal particles in Stardust tracks. The organics in several terminal particles were analyzed using IR spectroscopy during PET and these results will be published elsewhere. Nonetheless, one can compare the ratios of functional groups from the diffuse organics we see around tracks with those seen in stratospheric IDPs. In those tracks that show diffuse organics (tracks C2009,7,62 and C2009,4,59) the $-CH_2-/-CH_3$ functional group ratio is 2.0. These compare to a value of $CH_2/CH_3 \sim 3.7$ in a few terminal Stardust particles (Keller et al. 2006; Sandford et al. 2006). The -CH2-/-CH_3 functional group ratios are highly variable in IDPs, and show a larger range extending from as high as 8.4 down to 1.5, with an average value of about 3.6 (Flynn et al. 2003). Thus, both materials are fairly CH_2-rich compared to meteoritic insoluble organic material ($-CH_2CH_2-/-CH_3$ ~2.2, cf. Flynn et al. 2003) and organics in the diffuse interstellar medium ($-CH_2-/-CH_3$ ~2.5, cf. Sandford et al. 1991). At face value the IDPs and Stardust terminal particles appear to be more CH_2-rich than the organics surrounding Stardust tracks, but given the large variability of both populations and the limited statistics, it is not yet clear if this represents a significant difference.

One final caveat must be mentioned concerning the result presented here. While, as described before, we are reasonably confident that the diffuse halos of extra organic material we see around some tracks are associated with the impacting particles, one cannot be sure that the observed materials represent *unaltered* cometary material. Again, the hypervelocity impact collection of grains into aerogel involves the dissipation of considerable energy (Stratton and Szydlik 1997) and the localized heating of aerogel. This could have resulted in substantial alteration of any organics delivered by the original particle. A limited number of test shots of "standards" like simple PAHs and Allende into aerogel were made prior to the Stardust Preliminary Examination. These showed that aromatic species in these samples were not greatly changed during capture at velocities around 6 km/s, but that some species could be "injected" into

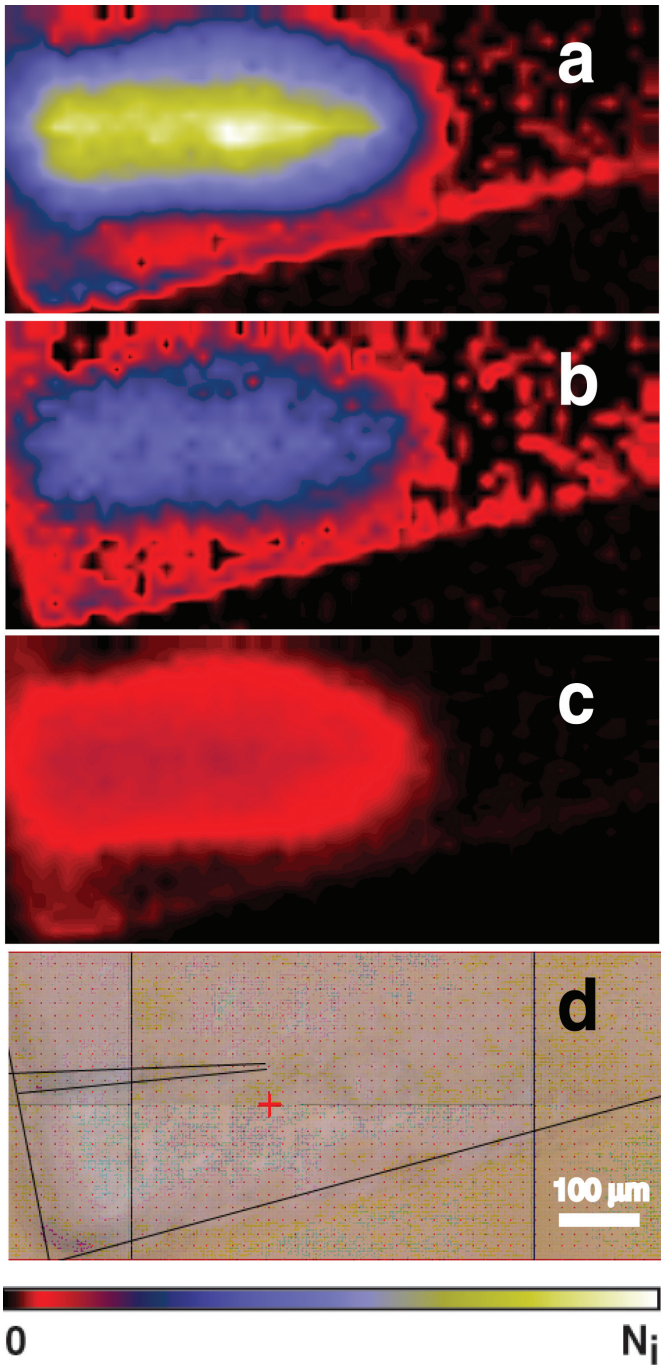

Fig. 9. Absorbance maps for -CH_2- (a), -CH_3 (b), and C=O (c) can be compared to the optical image (d) showing the edges of the keystone in sample C2009,4,59. The same false color bar is used in all three absorbance maps. Similar as in Fig. 6, the black color corresponds to 0 and white corresponds to a maximum functional density. We plot distribution of -CH_2- in Fig. 9a, -CH_3 in Fig. 9b and C=O in Fig. 9c. All four maps show identical area (same distance scale). Figure 9d is the optical image of the mapped area (approximately 750×350 μm^2). The original aerogel surface exposed to the comet is on the left. The two vertical black lines in the optical image (9d) are stitches of two images.

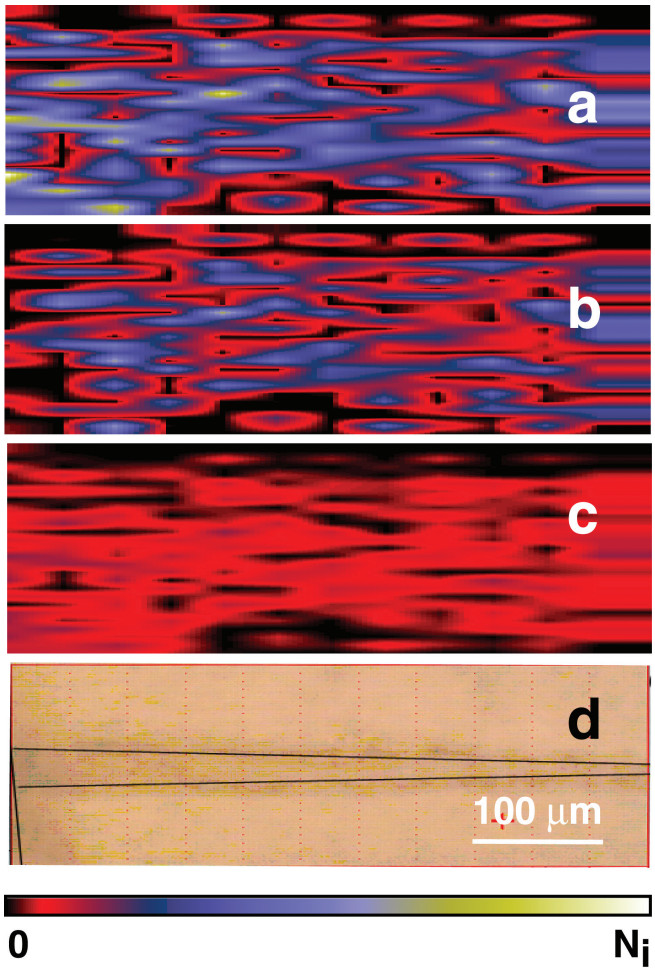

Fig. 10. Absorbance maps of -CH_2- (a), -CH_3 (b) and C=O (c) in track C2009,6,61. The optical image (Fig. 10d) of the track shows the aerogel surface exposed to the comet on the left. The mapped area is approximately 500×200 μm^2. The black color in the false color scale corresponds to 0 and white corresponds to a maximum functional density.

the aerogel surrounding the track. For example, the organics detected by L^{2}MS (two-step laser mass spectrometry) in Allende and several other carbonaceous chondrites were largely unchanged by capture in aerogel (Clemett et al., Forthcoming). Thus, current, limited data suggest aromatic species may be relatively "robust" with regards to this type of alteration. Not as much work has been done to address the issue of the alteration of less-aromatic species. In a test shot in which cocoa powder was fired into aerogel, the resulting material in the track was seen to contain vastly more aromatic species that the original sample, indicating that the impact had significantly altered the original material (Clemett, personal communication). This suggests that one of the consequences of impact processing may be to partially aromatize the sample. This would not directly explain the nature of the materials in halos around some Stardust tracks since the

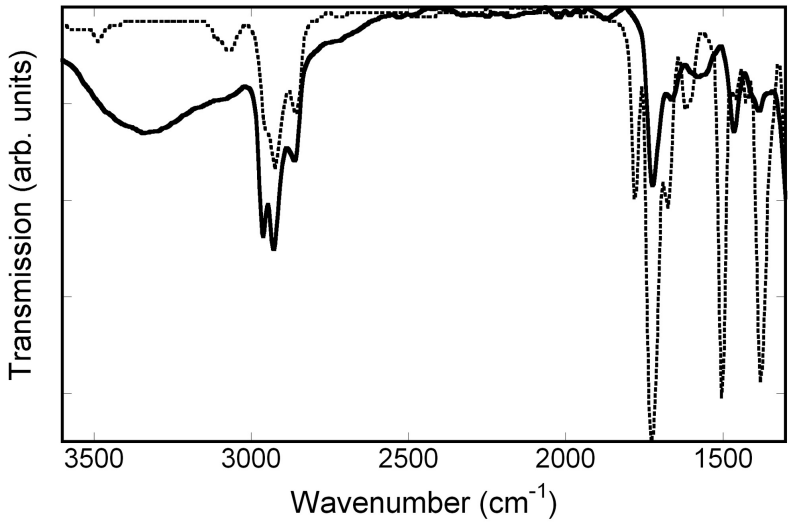

Fig. 11. Polyimide-Kapton (dash) versus volatile organics-rich Stardust aerogel (solid) spectrum. Note the absence of some strong peaks between 1300–1600 cm^{-1} in Stardust aerogel. The polyimide spectrum is taken from Omnic library (Omnic is a registered trademark of Thermo Electron Corporation). One tick interval on the y axis corresponds to 20% transmission.

materials we see are largely aliphatic, but this test serves to reinforce the caution that must be taken when interpreting the results of organic studies of Stardust samples. Clearly one cannot assume that all the cometary-based organics present in Stardust tracks are unaltered.

SUMMARY

Six particle tracks from two different aerogel cells (C2115 and C2009) have been examined using IR spectroscopy in this study. Infrared spectroscopy as a noninvasive technique proved to be ideal for preliminary studies (selecting interesting tracks/areas) of valuable materials, like Stardust samples, prior to any other type of analysis. Unexpected diffuse halos of organic material has been observed around three of the tracks (track C2115,22,20, track C2009,4,59, and track C2009,7,62). Two of these particle tracks came from cell C2009 and one from cell C2115. The excess volatile organic material was found to be $-CH_2-$ rich. Weaker bands of $-CH_3$, and C=O were also observed in this diffuse material. One possible explanation for these halos could be processing of carbon originally present in aerogel and modified due to high velocity impact. We argue that the presence of tracks with no excess organic materials, and the lack of observed depletion of original CH_3-rich aerogel carbon in our maps suggest that reprocessing of carbon indigenous to the aerogel is not likely to be the cause of the features we see. Another possible explanation of the excess organic material is contamination from Whipple shield (in off-normal incidence tracks). However, the spectra clearly do not match with the Kapton spectrum (Whipple shield material). The added organics in both off-normal and normal incidence tracks are the same indicating similar source for these materials.

Using corrected absorbance maps, we estimated the number of functional groups for a particular vibrational band in each track. "Organic rich" particle tracks have on average about an order of magnitude more organics than "organics poor" ones. It would be of great interest to compare these results with other Stardust tracks, either from the same or from other cells. The measurements reported in this paper were made during PET period (April and June 2006), within 3 to 6 months after the Stardust landing and sample exposure to the air. Re-mapping of these tracks should show if the volatile organics are stable in the air. Unfortunately, all the tracks discussed here have been "used up" for other analyses.

There is a lack of FTIR analysis on controlled laboratory impact experiments of different materials. Furthermore, alteration of carbon (organic materials) and its interaction with aerogel during the high velocity impact is not a well understood process and requires extensive additional work. As a practical advice for future analysis we recommend that the keystones are cut large enough so that a "clean aerogel" area can always be found beyond the outer extent of any "plume" of collected volatile organics. Nevertheless they need to remain thin enough to be transparent (usually up to 200 micron thick) for FTIR analysis.

Acknowledgments—We are grateful for support and samples provided by the NASA Stardust Discovery Mission and the NASA Stardust Participating Scientist Program. We thank H. N. Chapman (LLNL) for technical discussions and M. C. Martin (ALS, LBNL), Z. Hao (ALS, LBNL) and G. L. Carr, L. Miller and R. Smith (NSLS, BNL) for assistance with the experiments. Part of this work was performed under the auspices of the U.S. Department of Energy by the Lawrence Livermore National Laboratory under contract no. W-7405-ENG-48, the Advanced Light Source, Lawrence Berkeley

National Laboratory, which is supported by the Director, Office of Science, Office of Basic Energy Sciences, Materials Sciences Division, of the U.S. Department of Energy under contract no. DE-AC03-76F00098, and the National Synchrotron Light Source, Brookhaven National Laboratory, which is supported by U. S. Department of Energy, Division of Materials Sciences and Division of Chemical Sciences, under contract no. DE-AC02-98H10886. This paper benefited from the thoughtful comments of three anonymous reviewers.

Editorial Handling—Dr. Ian Franchi

REFERENCES

Bernstein M. P., Sandford S. A., Allamandola L. J., Gillette J. S., Clemett S. J., and Zare R. N. 1999. UV irradiation of polycyclic aromatic hydrocarbons in ices: Production of alcohols, quinones, and ethers. *Science* 283:1135–1138.

Bernstein M., Dworkin J., Sandford S., Cooper G., and Allamandola L. 2002. Racemic amino acids from the ultraviolet photolysis of interstellar ice analogues. *Nature* 416:401–403.

Brownlee D. E., Tsou P., Anderson J. D., Hanner M. S., Newburn R. L., Sekanina Z., Clark B. C., Hörz F., Zolensky M. E., Kissel J., McDonnell J. A. M., Sandford S. A., and Tuzzolino A. J. 2003. Stardust: Comet and interstellar dust sample return mission. *Journal of Geophysical Research* 108(E10)8111:1-1–1-15.

Brownlee D., Tsou P., Aléon J., Alexander C. M. O'D., Araki T., Bajt S., Baratta G. A., Bastien R., Bland P., Bleuet P., Borg J., Bradley J. P., Brearley A., Brenker F., Brennan S., Bridges J. C., Browning N., Brucato J. R., Brucato H., Bullock E., Burchell M. J., Busemann H., Butterworth A., Chaussidon M., Cheuvront A., Chi M., Cintala M. J., Clark B. C., Clemett S. J., Cody G., Colangeli L., Cooper G., Cordier P., Daghlian C., Dai Z., D'Hendecourt L., Djouadi Z., Dominguez G., Duxbury T., Dworkin J. P., Ebel D., Economou T. E., Fairey S. A. J., Fallon S., Ferrini G., Ferroir T., Fleckenstein H., Floss C., Flynn G., Franchi I. A., Fries M., Gainsforth Z., Gallien J.-P., Genge M., Gilles M. K., Gillet P., Gilmour J., Glavin D. P., Gounelle M., Grady M. M., Graham G. A., Grant P. G., Green S. F., Grossemy F., Grossman L., Grossman J., Guan Y., Hagiya K., Harvey R., Heck P., Herzog G. F., Hoppe P., Hörz F., Huth J., Hutcheon I. D., Ishii H., Ito M., Jacob D., Jacobsen C., Jacobsen S., Joswiak D., Kearsley A. T., Keller L., Khodja H., Kilcoyne A. L. D., Kissel J., Krot A., Langenhorst F., Lanzirotti A., Le L., Leshin L., Leitner J., Lemelle L., Leroux H., Liu M.-C., Luening K., Lyon I., MacPherson G., Marcus M. A., Marhas K., Matrajt G., Meibom A., Mennella V., Messenger K., Mikouchi T., Mostefaoui S., Nakamura T., Nakano T., Newville M., Nittler L. R., Ohnishi I., Ohsumi K., Okudaira K., Papanastassiou D. A., Palma R., Palumbo M. E., Pepin R. O., Perkins D., Perronnet M., Pianetta P., Rao W., Rietmeijer F., Robert F., Rost D., Rotundi A., Ryan R., Sandford S. A., Schwandt C. S., See T. H., Schlutter D., Sheffield-Parker J., Simionovici A., Simon S., Sitnitsky I., Snead C. J., Spencer M. K., Stadermann F. J., Steele A., Stephan T., Stroud R., Susini J., Sutton S. R., Taheri M., Taylor S., Teslich N., Tomeoka K., Tomioka N., Toppani A., Trigo-Rodríguez J. M., Troadec D., Tsuchiyama, A. Tuzolino A. J., Tyliszczak T., Uesugi K., Velbel M., Vellenga J., Vicenzi E., Vincze L., Warren J., Weber I., Weisberg M., Westphal A. J., Wirick S., Wooden D., Wopenka B., Wozniakiewicz P., Wright I., Yabuta H., Yano H., Young E. D., Zare R. N., Zega T., Ziegler K., Zimmerman L., Zinner E., and Zolensky M. E. 2006. Comet 81P/Wild 2 under a microscope. *Science* 314:1711–1716.

Burchell M. J., Graham G., and Kearsley A. 2006. Cosmic dust collection in aerogel. *Annual Reviews of Earth and Planetary Sciences* 34:385–418.

Carr G. L., Merlo O., Munsli M., Springer S., and Ho S. C. 1999. Characterization of the new NSLS infrared microspectroscopy beamline U10B. In *Accelerator-based sources of infrared and spectroscopic applications*, edited by Carr G. Lawrence and Dumasy P. Proceedings of SPIE, vol. 3775. Bellingham, Washington: The Society of Photo-Optical Engineers. pp. 22–29.

Clemett S. J., Sandford S., Nakamura-Messenger K., Hörz F., and McKay D. Forthcoming. Complex aromatic hydrocarbons in Stardust samples collected from comet 81P/Wild 2. *Meteoritics & Planetary Science*.

Cody G. D., Ade H., Alexander C. M. O'D., Araki T., Butterworth A., Fleckenstein H., Flynn G., Gilles M. K., Jacobsen C., Kilcoyne A. L. D., Messenger K., Sandford S. A., Tyliszczak T., Westphal A. J., Wirick S., and Yabuta H. 2008. Quantitative organic and light-element analysis of comet 81P/Wild 2 particles using C-N-, and O- μ-XANES. *Meteoritics & Planetary Science* 43:353–365.

Dartois E., Marco O., Muñoz-Caro G. M., Brooks K., Deboffle D., D'Hendecourt L. 2004. Organic matter in Seyfert 2 nuclei: Comparison with our galactic center lines of sight. *Astronomy and Astrophysics* 423:549–558.

Ehrenfreund P., Robert F., D'Hendencourt L., and Behar F. 1991. Comparison of interstellar and meteoritic organic-matter at 3.4 μm. *Astronomy and Astrophysics* 252:712–717.

Flynn G., Bleuet P., Borg J., Bradley J. P., Brenker F. E., Brennan S., Bridges J., Brownlee D. E., Bullock E. S., Burghammer M., Clark B. C., Dai Z. R., Daghlian C. P., Djouadi Z., Fakra S., Ferroir T., Floss C., Franchi I. A., Gainsforth Z., Gallien J. P., Gillet P., Grant P. G., Graham G. A., Green S. F., Grossemy F., Heck P. R., Herzog G. F., Hoppe P., Hörz F., Huth J., Ignatyev K., Ishii H. A., Janssens K., Joswiak D., Kearsley A. T., Khodja H., Lanzirotti A., Leitner J., Lemelle L., Leroux H., Luening K., MacPherson G. J., Marhas K. K., Marcus M. A., Matrajt G., Nakamura T., Nakamura-Messenger K., Nakano T., Newville M., Papanastassiou D. A., Pianetta P., Rao W., Riekel C., Rietmeijer F. J. M., Rost D., Schwandt C. S., See T. H., Sheffield-Parker J., Simionovici A., Sitnisky I., Snead C. J., Stadermann F. J., Stephan T., Stroud R. M., Susini J., Susuki Y., Sutton S. R., Taylor S., Teslich N., Troadec D., Tsou P., Tsuchiyama A., Uesigi K., Vekemans B., Vicenzi E. P., Vincze L., Westphal A. J., Wosniakiewicz P., Zinner E., and Zolensky M. E. 2006. Elemental compositions of comet 81P/Wild 2 samples collected by Stardust. *Science* 314:1731–1735.

Flynn G. J., Keller L. P., Feser M., Wirick S., and Jacobsen C. 2003. The origin of organic matter in the solar system: Evidence from the interplanetary dust particles. *Geochimica et Cosmochimica Acta* 67:4791–4806.

Flynn G. J., Keller L. P., Jacobsen C., and Wirick S. 2004. An assessment of the amount and types of organic matter contributed to the Earth by interplanetary dust. *Advances in Space Research* 33:57–66.

Holman H.-Y. and Martin M. C. 2006. Synchrotron radiation infrared spectromicroscopy: A non-invasive chemical probe for monitoring biogeochemical processes. *Advances in Agronomy* 90:79–127.

Hörz F., Bastien R., Borg J., Bradley J. P., Bridges J. C., Brownlee D. E., Burchell M. J., Chi M., Cintala M. J., Dai Z. R., Djouadi Z., Dominguez D., Economou T. E., Fairey S. A. J., Floss C., Franchi I. A., Graham G. A., Green S. F., Heck P., Hoppe P., Huth J., Ishii H., Kearsley A. T., Kissel J., Leitner J., Leroux H., Marhas K., Messenger K., Schwandt C. S., See T. H., Snead C., Stadermann F. J., Stephan I. T., Stroud R., Teslich N., Trigo-Rodríguez J. M., Tuzzolino A. J., Troadec D., Tsou P., Warren J., Westphal A., Wozniakiewicz P., Wright I., and Zinner E. 2006.

Impact features on Stardust: Implications for comet 81P/Wild 2 dust. *Science* 314:1716–1719.

Keller L. P., Bajt S., Baratta G. A., Borg J., Bradley J. P., Brownlee D. E., Brucato J. R., Burchell M. J., Busemann H., Colangeli L., D'Hendecourt L., Djouadi Z., Ferrini G., Flynn G., Franchi I. A., Fries M., Grady M.M., Gilles M. K., Graham A., Grossemy F., Kearsley A., Matrajt G., Nakamura-Messanger K., Mennella V., NittlerL. R., Palumbo M. E., Rotundi A., Sandford S.A., Snead C. J., Stadermann F. J., Steele A., Tsou P., Wooden D., and Zolensky M. 2006. Infrared spectroscopy of comet 81P/Wild 2 samples returned by Stardust. *Science* 314:1728–1731.

Matrajt G., Muñoz Caro G. M., Dartois E., D'Hendecourt L., Deboffle D., and Borg J. 2005. FTIR analysis of the organics in IDPs: Comparison with the IR spectra of the diffuse interstellar medium. *Astronomy and Astrophysics* 433:979–995.

Matrajt G., Ito M., Wirick S., Brownlee D. E., Joswiak D., Flynn G., Sandford S., Snead C., and Westphal A. 2008. Carbon investigation of Stardust particles: A TEM, NanoSIMS and XANES study. *Meteoritics & Planetary Science* 43:315–334.

McKeegan K. D., Aléon J., Bradley J., Brownlee D., Busemann H., Butterworth A., Chaussidon M., Fallon S., Floss C., Gilmour J., Gounelle M., Graham G., Guan Y., Heck P. R., Hoppe P., Hutcheon I. D., Huth J., Ishii H., Ito M., Jacobsen S. B., Kearsley A., Leshin L. A., Liu M.-C., Lyon I., Marhas K., Marty B., Matrajt G., Meibom A., Messenger S., Mostefaoui S., Mukhopadhyay S., Nakamura-Messenger K., Nittler L., Palma R., Pepin R. O., Papanastassiou D. A., Robert F., Schlutter D., Snead C. J., Stadermann F. J., Stroud R., Tsou P., Westphal A., Young E. D., Ziegler K., Zimmermann L., and Zinner E. 2006. Isotopic compositions of cometary matter returned by Stardust. *Science* 314:1724–1727.

Mennella V., Brucato J. R., Colangeli L., and Palumbo P. 2002. C-H bond formation in carbon grains by exposure to atomic hydrogen: The evolution of the carrier of the interstellar 3.4 micron band. *The Astrophysical Journal* 569:531–540.

Moultaka J., Eckart A., Viehmann T., Mouawad N., Straubmeier C., Ott T., and Schödel R. 2004. Dust embedded sources at the galactic center. 2 to 4 μm imaging and spectroscopy in the central parsec. *Astronomy and Astrophysics* 425:529–542.

Muñoz-Caro G. M., Meierhenrich U., Schutte W., Barbier B., Arcones Segovia A., Rosenbauer H., Thiemann W., Brack A., and Greenberg J. 2002. Amino acids from ultraviolet irradiation of interstellar ice analogues. *Nature* 416:403–406.

Pendelton Y. J., Sandford S. A., and Allamandola L. J. et al. 1994. Near-infrared absorption-spectroscopy of interstellar hydrocarbon grains. *The Astrophysical Journal* 437:683–696.

Rotundi A., Baratta G. A., Borg J., Brucato J. R., Busemann H., Colangeli L., D'Hendecourt L., Djouadi Z., Ferrini G., Franchi I. A., Fries M., Grossemy F., Keller L. P., Mennella V., Nakamura K., Nittler L. R., Palumbo M. E., Sandford S. A., Steele A., and Wopenka B. 2008. Combined micro-Raman, micro-Infrared, and field emission scanning electron microscope analyses of comet 81P/Wild 2 particles collected by Stardust. *Meteoritics & Planetary Science* 43:367–397.

Sandford S. A., Allamandola L. J., Tielens A. G. G. M., Sellgren K., Tapia M., and Pendelton Y. 1991. The interstellar C-H stretching band near 3.4 microns: Constraints on the composition of organic material in the diffuse interstellar medium. *The Astrophysical Journal* 371:607–620.

Sandford S. A., Pendelton Y. J., and Allamandola L. J. 1995. The galactic distribution of aliphatic-hydrocarbons in the diffuse interstellar-medium. *The Astrophysical Journal* 440:697–705.

Sandford S. A., Aléon J., Alexander C. M. O'D., Araki T., Bajt S., Baratta G. A., Borg J., Bradley J. P., Brownlee D. E., Brucato J. R., Burchell M. J., Busemann H., Butterworth A., Clemett S. J., Cody G., Colangeli L., Cooper G., D'Hendecourt L., Djouadi Z., Dworkin J. P., Ferrini G., Fleckenstein H., Flynn G. J., Franchi I. A., Fries M., Gilles M. K., Glavin D. P., Gounelle M., Grossemy F., Jacobsen C., Keller L. P., Kilcoyne A. L. D., Leitner J., Matrajt G., Meiborn A., Mennelle V., Mostefaoui S., Nittler L.R., Palumbo M. E., Papanastassiou D. A., Robert F., Rotundi A., Snead C. J., Spencer M. K., Stadermann F. J., Steele A., Stephan T., Tsou P., Tyliszczak T., Westphal A. J., Wirick S., Wopenka B., Yabuta H., Zare R. N., and Zolensky M. E. 2006. Organics captured from comet 81P/Wild 2 by the Stardust spacecraft. *Science* 314:1720–1724.

Sandford S. A. and Brownlee D. E. 2007. Response to comment on "Organics captured from comet 81P/Wild 2 by the Stardust spacecraft." *Science* 317:1680d.

Spencer M. K. and Zare R. N. 2007. Comment on "Organics captured from comet 81P/Wild 2 by the Stardust spacecraft." *Science* 317: 1680c.

Spencer M. K., Clemett S. J., Sandford S. A., McKay D. S., and Zare R. N. 2009. Organic compound detection along hypervelocity particle impact tracks in Stardust aerogel. *Meteoritics & Planetary Science* 44:15–24.

Stratton D. M. and Szydlik O. P. 1997. Modeling the capture of cosmic dust particles in aerogel (abstract #1164). 28th Lunar and Planetary Science Conference.

Tsou P. 1995. Silica aerogel captures cosmic dust intact. *Journal of Non-Crystalline Solids* 186:415–427.

Tsou P., Brownlee D. E., Sandford S. A., Hörz F., and Zolensky M. E. 2003. Wild 2 and interstellar sample collection and Earth return. *Journal of Geophysical Research* 108:3-1–3-21.

Westphal A. J., Snead C., Butterworth A., Graham G. A., Bradley J. P., Bajt S., Grant P., Bench G., Brennan S., and Pianetta P. 2004. Aerogel keystones: Extraction of complete hypervelocity impact events from aerogel collectors. *Meteoritics & Planetary Science* 39:1375–1386.

Westphal A. J., Bastien R. K., Borg J., Bridges J., Brownlee D. E., Burchell M. J., Cheng A. F., Clark B. C., Djouadi Z., Floss C., Franchi I., Gainsforth Z., Graham G., Green S. F., Heck P. R., Horanyi M., Hoppe P., Hörz F. P., Huth J., Kearsley A., Leroux H., Marhas K., Nakamura-Messenger K., Sandford S. A., See T. H., Stadermann F. J., Teslich N. E., Tsitrin S., Warren J. L., Wozniakiewicz P. J., and Zolensky M. E. 2008. Discovery of non-random spatial distribution of impacts in the Stardust cometary collector. *Meteoritics & Planetary Science* 43:415–429.

Wexler A. S. 1967. Integrated intensities of absorption bands in infrared spectroscopy. *Applied Spectroscopy Review* 1:29–98.

Yelle R. V., Soderblom L. A., and Jokipii R. J. 2004. Formation of jets in comet 19P/Borrelly by subsurface geysers. *Icarus* 167:30–36.

Zolensky M. E., Zega T. J., Yano H., Wirick S., Westphal A. J., Welsberg M. K., Weber I., Warren J. L., Velbel M. A., Tsuchiyama A., Tsou P., Toppani A., Tomioka N., Kazuchige T., Teslich N., Taheri M., Susini J., Stroud R., Stephan T., Staderman F. J., Snead C. J., Simon S. B., Simionovici A., See T. H., Robert F., Rietmeijer F. J., Rao W., Perronnet M. C., Nakamura-Messenger K., Nakamura T., Mostefaoui S., Mikouchi T., Melbom A., Matrajt G., Marcus M. A., Leroux H., Lemelle L., Le L., Lanzirotti A., Langenhorst F., Krot A. N., Keller L. P., Kearsley A.T., Joswiak D., Jacob D., Ishii H., Harvey R., Hagiya K., Grossman L., Grossman J. N., Graham G. A., Gounelle M., Gillet P., Genge M. J., Flynn G., Ferroir T., Fallon S., Ebel D. S., Dai Z.R., Cordier P., Clark B., Chi M., Butterworth A. L., Brownlee D. E., Bridges J. C., Brennan S., Brearley A., Bradley J. P., Bleuet P., Bland P. A., and Bastien R. 2006. Mineralogy and petrology of comet 81P/Wild 2 nucleus samples. *Science* 314:1735–1739.